NIPPON STEEL TECHNICAL REPORT No. 104 AUGUST 2013

Technical Report

UDC 621 . 746 . 049 : 53 . 072

Clarification and Control of the Heat Transfer Phenomenon in the Mold and Strand of Continuous Casting Machines

Hideaki YAMAMURA*
Toshiyuki KAJITANI
Junji NAKASHIMA
Norimasa YAMASAKI
Satoru MINETA

Abstract

The heat transfer phenomena in the mold and the strand of continuous casting machine were examined and control technologies were considered. The heat transfer phenomenon through the mold flux film in the mold was examined by the heat transfer measurement experimental apparatus. The cold model experiment that simulate the infiltration of mold flux and the numerical analysis model using the Reynolds equation was developed, and the mechanism of the mold flux infiltration that give the great influence to the heat transfer and the lubrication in the mold was considered. In addition, the mechanism of the hydrogen induced break out was clarified by measurement of the content of OH^- radical in mold flux by ^1H solid NMR device, and the countermeasures were considered. Furthermore, the FEM model which analyzed the deformation behavior of the solidification shell was developed, and the influence of the mold shape to uniformity of the solidification shell was studied. The numerical analysis model that simulate the behavior of the water in the secondary cooling of strand was developed using a particle method, and the influence of the leak water from the gap between the bearing of sprit roll and the cast slab and the stagnant water in the wedge-shaped space formed by the roll and the slab was examined.

1. Introduction

With an increase in continuous casting speed, the occurrence of defects such as surface cracks, and nonmetallic inclusions, the instability of casting operation such as mold level fluctuations, and breakouts become increasingly conspicuous. In order to prevent the occurrence of slab surface cracks and breakouts, in particular, during high-speed continuous casting operation, it is critical to ensure the formation of a uniformly solidified shell by controlling heat transfer and cooling of the molten steel in the mold and strand and also to maintain the mold in the proper lubrication condition. Additionally, an unevenly solidified shell at the final stage of solidification in the strand aggravates the incidence of slab centerline segregation. In order to solve these problems, it is necessary to obtain a clear appreciation of the behavior of mold flux and the phenomenon of heat removal in the mold and to control the infiltration of mold flux in between the mold and the solidified shell and the heat flux through the flux film. In addition, it is important to ensure uniform heat removal by secondary cooling of the strand.

In this report, we make an attempt to clarify the phenomenon of heat transfer in the mold and strand and utilize the resulting understanding to suggest techniques to control the phenomenon for the betterment of high-speed continuous casting processes.

2. Heat Transfer and Infiltration Behavior of Mold Flux

2.1 Mechanism of heat transfer through flux film [1)]

Many reports have been published on the heat transfer through the flux film and interface between the mold and flux film as well as on the influence of the crystallization of solidified flux on the heat transfer phenomenon.[2-6)] However, few of those reports evaluate the contribution to the phenomenon of both the liquid and solid phases of the film and the interface between the solid phase and the mold.

* Chief Researcher, Steelmaking R&D Div., Process Technology Center
20-1 Shintomi, Futtsu, Chiba 293-8511

Therefore, we carried out an experiment simulating the behavior of heat transfer between the solidified shell and the mold through the flux film in order to quantitatively evaluate the influence of each of the above elements. In addition, we studied the factors that govern the heat transfer during a continuous casting operation by comparing the structure of flux film obtained from an actual continuous casting machine.

Using the experimental apparatus shown in **Fig. 1**, a mold flux having a basicity of 1.1 was melted in a steel crucible heated to 1,450 ˚C. After that, a water-cooled copper block was lowered until the flux film between the steel crucible and the copper block reached the prescribed thickness, at which point the copper block was held in position. The flux temperature was measured with thermocouples installed in both the steel crucible and the water-cooled copper block. In addition, in order to examine the microstructure of the film under experimentation, the flux film was pulled up together with the water-cooled copper block after the experiment and cooled rapidly. From examination of the cross-sectional microstructure of the collected flux film sample, the thicknesses of the solid and liquid phases of the film were determined. From the measured temperature and thickness of each of the phases, the overall thermal resistance between the steel crucible and the water-cooled copper block, the thermal resistance of the solid phase and the liquid phase and the thermal resistance at the interface between the steel crucible and the solid phase of the film were obtained.

Fig. 2 shows a cross section of the flux film composed of a liquid and a solid phase. The solid phase accounts for the greater part, roughly 80% to 90%, of the film and consists mainly of crystals.

Fig. 3 shows the change in the thermal resistance of the solid phase, liquid phase, and the interface between the mold and the solid

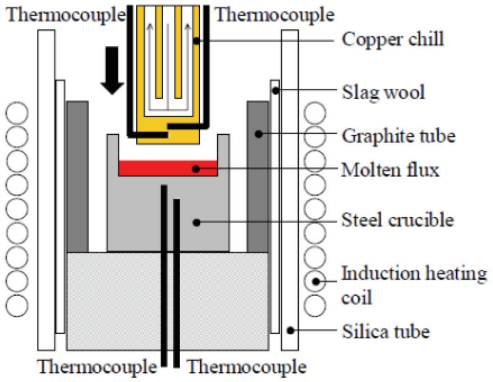

Fig. 1 Schematic illustration of experimental apparatus

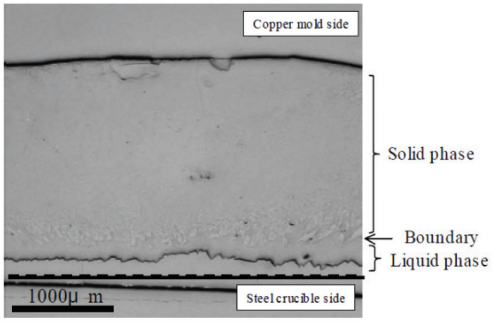

Fig. 2 Cross section of mold flux film (2mm in thickness)

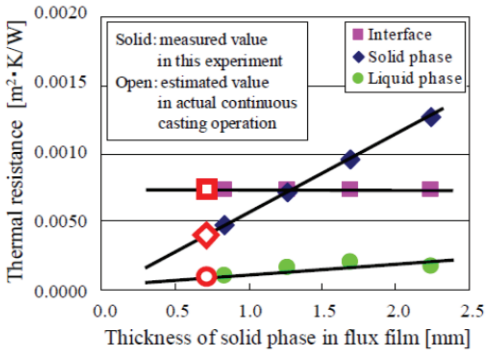

Fig. 3 Thermal resistance of each phase in the mold flux film as a function of thickness of solid phase in flux film

phase according to a change in film thickness. The liquid phase displays a lower thermal resistance than either the solid phase or the interface between the mold and the solid phase. With increasing film thickness, the thermal resistance of the solid phase increases but that of the interface remains almost the same. Therefore, from this analysis, it can be concluded that, when the solid phase thickness is 1.3 mm or less, the thermal resistance of the interface is predominant, whereas, when the solid phase thickness is more than 1.3 mm, the thermal resistance of the solid phase becomes predominant. The solid phase thickness of a film collected from the mold of an actual continuous caster was 0.7 mm.[7] This fact suggests that the factor governing the heat transfer between the solidified shell and the mold in an actual continuous caster is the thermal resistance at the interface between the mold and the flux film. Therefore, in order to lower the cooling rate of the mold, it is effective to promote the infiltration of flux and thereby increase the thickness of the flux film.

2.2 The mechanism of flux infiltration[8-11]

As described above, the infiltration of flux is important not only for lubrication but also for heat transfer in the mold. Many studies have reported the mechanism of flux infiltration.[12, 13] Nevertheless, even with regards to the timing of the infiltration of molten flux—whether it is the negative strip time or the positive strip time, there is still a difference of opinion. On the other hand, reports have been published on theoretical analyses[14] and model experiments[15] dealing with the behavior of the infiltration of molten flux between the mold and the solidified shell. However, most of these reports assume that the distance between the mold and the solidified shell is invariable. In this respect, it can hardly be said that they reproduce the actual phenomena.

Therefore, on the assumption that the thickness of flux film can vary during casting according to the balance between the molten steel static pressure acting upon the solidified shell and the pressure inside the flux film, we have made an attempt to clarify the mechanism of the infiltration of mold flux by a model experiment and a theoretical analysis.

Fig. 4 schematically shows the apparatus used for the model experiment. Silicone oil was fed into the gap between a turning belt and an acrylic plate capable of freely moving horizontally. The acrylic plate surface was given a 0.5-degree taper against the vertical direction to ensure a downward spreading admission of the flux. In addition, to simulate mold oscillation, the belt turning speed was periodically altered. To simulate the molten steel static pressure acting on the unconstrained solidified shell within a continuous casting mold process, constant pressure was applied to the back of the

acrylic plate by using an air cylinder. The horizontal displacement of the acrylic plate was measured with a contact-type displacement gauge.

The change in oil film thickness with respect to the time-serial change in belt speed is shown in **Figs. 5**(a) and (b). The film thickness was found to change in accordance with a change in belt speed: it increased when the belt speed increased and decreased when the belt speed decreased. While repeating that process, the oil flowed downward. The time during which the oil flows downward corresponds to the time from the second half of the positive strip time to the second half of the negative strip time of the mold oscillation in a continuous casting process.

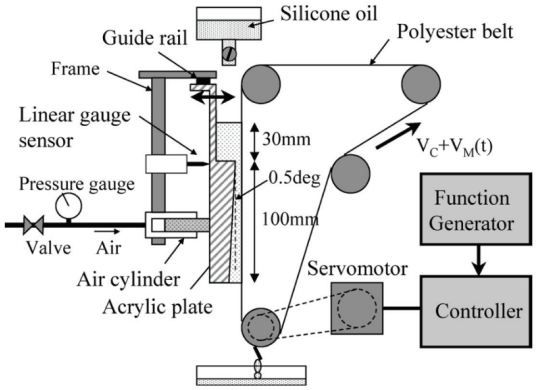

Fig. 4 Schematic illustration of cold model experiment

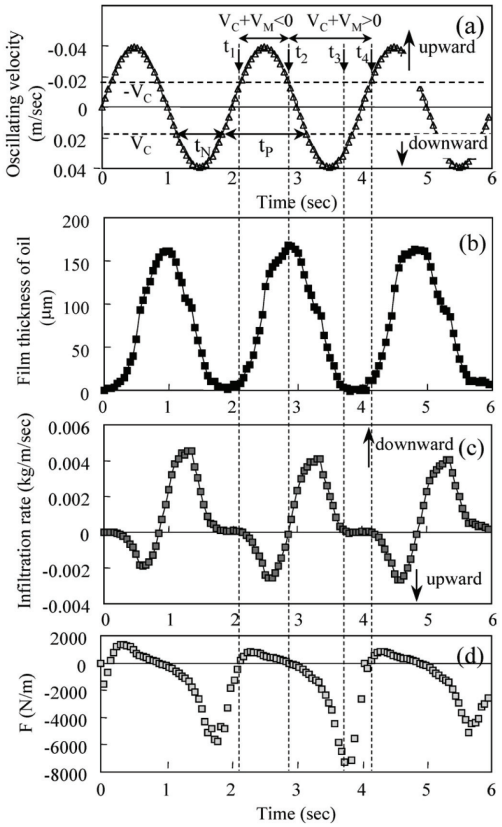

Fig. 5 Oscillating velocity of the belt (a), film thickness of silicone oil at the channel entrance (b), infiltration rate (c) and force acting on the acrylic plate (d) as a function of time. V_C = 1.0 m/min, frequency of oscillation = 0.5 Hz, stroke of oscillation = 25 mm, kinematic viscosity of oil = 500 cs

The oil infiltration rate, calculated from film thickness, is shown in Fig. 5(c). While the oil flows both downward and upward according to the belt oscillation, on the whole, the oil was found to flow downward. Paying attention to a single period, the oil flows upward from t_1 to t_2 for which $[V_C + V_M]$ is negative, whereas the oil flows down during the time from t_2 when $[V_C + V_M]$ becomes positive to t_3 when the channel closes. Thus, the time $(t_2 - t_3)$ during which the oil flows in is neither t_P nor t_N, but, rather, corresponds to the time for which the oil channel is open and $[V_C + V_M]$ is positive, that is, the time from the second half of the positive strip time to the second half of the negative strip time.

Pressure, F, inside the film, calculated from film thickness, is shown in Fig. 5(d). While the belt is moving up rapidly, F is positive, producing a force that moves the acrylic plate away from the belt. Therefore, the film thickness increases sharply in this period. Conversely, while the belt is moving down, F becomes negative, producing a force that draws the acrylic plate toward the belt. As a result, the film thickness decreases or is kept to zero.

From the above analysis, the behavior of the infiltration of mold flux by oscillations can be explained as follows. Between t_1 and t_2, the mold moves up, causing the film thickness to increase. Then, as the mold moves down, the flux rapidly flows in, spreading downward. With the rapid infiltration of flux, the pressure inside the flux film drops and the film thickness decreases. As a result, the rate of flux infiltration declines sharply. Through repetitions of the process, the mold flux is supplied between the mold and the solidified shell.

A flux infiltration model was created that takes the above phenomena into consideration. The basic equations are the Reynolds equation (1) and the equation of motion of the solidified shell (2). Using these two equations, the horizontal motion of the solidified shell was calculated dynamically.

$$\frac{\partial}{\partial x}\left[\frac{\rho h^3}{12\mu}\left(\frac{\partial P}{\partial x}-\rho g\right)\right]=\frac{V_C+V_0}{2}\frac{\partial \rho h}{\partial x}+\rho\frac{\partial h}{\partial t} \quad (1)$$

$$M\frac{d^2h}{dt^2}+B\frac{dh}{dt}+Kh=\int_0^L pdx \quad (2)$$

where, ρ denotes the density; μ, the viscosity; h, the distance between the mold and the solidified shell slab; P, the pressure; x, the distance in the casting direction; g, the gravitational acceleration, V_C, the casting speed; V_0, the oscillation speed; t, the time; and L, the length of the molten flux filled zone. Finally, the constants M, B, and K were used as adjustable fitting parameters.

Using the above model, we studied the influence of each of the various factors in a continuous casting process. As an example, the calculated influence of viscosity on flux consumption is shown in **Fig. 6**. With an increase in viscosity, the consumption of flux decreases. This calculation result agrees well with the results of measurement.

Based on the calculated effects of the factors regulating the infiltration of flux, it was confirmed that the amount of flux infiltration decreases with an increase in viscosity, casting speed, and oscillation frequency.

2.3 Hydrogen-induced breakouts [16)]

From the standpoint of ensuring a stable continuous casting operation, preventing breakouts (BO) is one of the most important challenges. The incidence of BO varies according to the season and the steel grade. It has been known empirically that the occurrence of

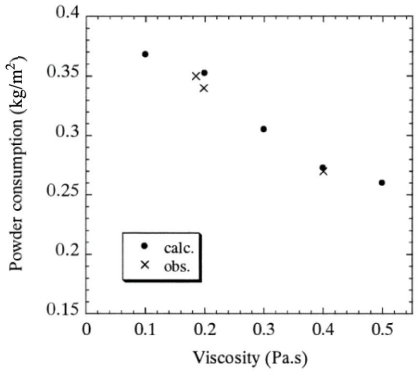

Fig. 6 Influence of viscosity on mold powder consumption

BO is especially high in the summertime. This has been ascribed to a rise in the hydrogen content of the molten steel caused by the entry of hydrogen from the atmosphere, refractories, and slag during the continuous casting operation.[17-19] From the standpoint of steel grades, Si-killed steel is especially susceptible to the sticking-type BO caused by hydrogen.

During continuous casting of Al-killed steel and Si-killed steel, mold flux films were collected and their cross sections compared. The microstructures of the cross sections are shown in **Fig. 7**.[16] There is evidence of many micropores in the films collected from the Si-killed steel process. It is suggested that the observed micropores influence the initial solidification and the flux infiltration via heat transfer in the mold, which eventually leads to BO.

It is surmised that micropores house water vapor and other gases that contain hydrogen atoms. To test this hypothesis, the concentrations of hydroxyl (OH) radical in the mold flux films were measured with ^{1}H solid NMR equipment.[20] The measurement results are shown in **Fig. 8**. In the molten slag of Si-killed steel, OH radical are concentrated. The reason for this is that, during the casting operation, the molten flux reacts with water vapor in the atmosphere and absorbs it in the form of OH^-, whereas the rise in concentration of OH^- in the molten slag of Al-killed steel is not very high since the OH^- containing slag reacts with Al in the molten steel and moves into the molten steel in the form of hydrogen. On the other hand, in the case of Si-killed steel, it was estimated that because of the small Al content of molten steel, OH^- is accumulated in the molten slag till it becomes saturated, and that after the slag flows in between the mold and the solidified shell, with decrease in temperature, OH^- becomes vapor and a bubble generals it in molten.

From consideration of the above mechanism, it was considered possible to facilitate the movement of hydrogen from the molten slag into the molten steel by promoting the reaction using a powder of high basicity and low SiO_2. Specifically, as shown in **Fig. 9**, a mold flux of high basicity is found to reduce the concentration of OH^- in the flux film and restrain the occurrence of micropores, thereby making it possible to reduce the incidence of BO.

Molten steel that is not degassed has a high concentration of hydrogen.[19] In this case, as the soluble hydrogen concentration decreases during solidification of the molten steel, the discharged hydrogen enters the molten flux film in the form of a gas. While micropores are not observed in the film of degassed molten steel collected from a mold, many micropores are observed in the film of non-degassed molten steel when the hydrogen concentration of the steel is 6 ppm or more.[21] From a model analysis of the release of hydrogen gas and the formation of hydrogen micropores during solidification of the molten steel, a relationship between the high-limit hydrogen concentration and casting speed/powder viscosity relative to the prevalence of BO was derived. As reported by Pontoire et al.,[18] the above mentioned model analysis confirmed that, when the hydrogen concentration is 8 ppm or more, the possibility of BO increases markedly depending on the casting speed and flux viscosity.[21]

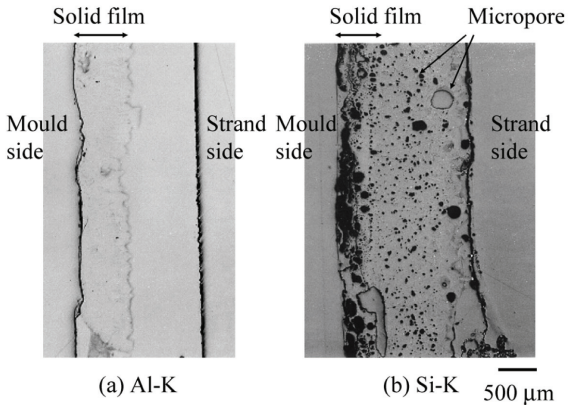

Fig. 7 Cross-section of a mold flux film detached from mould wall after casting of (a) Al−K and (b) Si−K steels

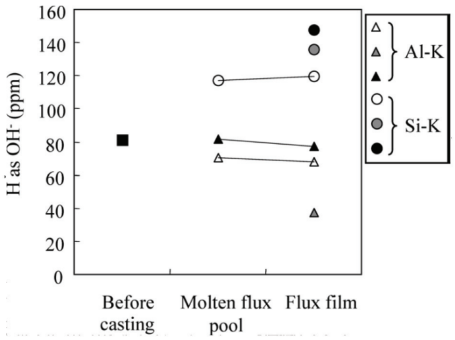

Fig. 8 Change in hydrogen as OH^- in mold flux during continuous casting

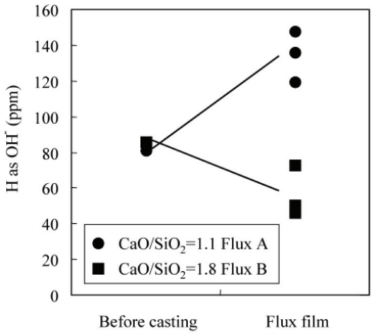

Fig. 9 Influence of basicity (CaO/SiO_2) on the change in hydrogen as OH^- in mold flux during the casting of Si−K steel

3. Control of Initial Solidification Using Suitable Mold Shapes and Electromagnetic Force and Control of Solidification in Strand by Secondary Cooling

The incidence of BO not only causes a major barrier for produc-

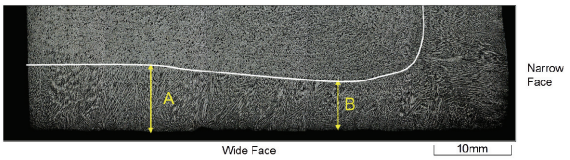

Fig. 10 Microstructure of shell around the corner just before break out

tion and equipment damage but also limits the productivity enhancement afforded by casting speed increase. A detailed examination of a slab after a BO revealed that the solidified shell around the corner of the mold had decreased in thickness (shell thickness B < shell thickness A) as shown in **Fig. 10**.

As a measure to prevent the problem caused by uneven solidification mentioned above, it is effective to control the initial solidification of molten steel by using a suitable mold shape and electromagnetic force. Using numerical analysis models and observing actual slabs, we examined the mechanisms of initial solidification of molten steel and studied the effects of a suitable mold shape and the use of electromagnetic force to control the initial solidification.

Controlling the solidification of molten steel in the strand under the mold is also important. Various measures are taken to minimize transverse corner cracking, internal cracking, and centerline segregation/porosity—the representative defects of slabs. Here, the contribution of secondary cooling to uneven growth of the solidification shell was studied by an analysis with an emphasis on the behavior of secondary cooling water.

3.1 Controlling initial solidification by using a suitable mold shape

Most of the conventional structural analyses for grasping the growth behavior of the solidified shell use a non-steady method in which the coordinate system is fixed to the unit cell of a slab. This method calculates temperatures and stresses while changing the surrounding boundary conditions on a time-serial basis. However, it does not permit taking into consideration the temperature and stress gradients in the casting direction. Therefore, another method that takes the visco-plastic behavior into consideration and that conducts the analysis in a velocity field under a space-fixed coordinate system, as in the rigid-plastic rolling analysis, was proposed.[22] However, the proposed model was two-dimensional, based on the generalized plane strain, and was insufficient to express cracks that occur in actual slabs. To rectify this limitation, a three-dimensional FEM analysis model that takes into account phase transformation, including mass transfer and solidification, thermal shrinkage, and visco-plastic behavior was developed.

(1) Model for the calculation of solidification

There are various methods of calculating solidification, such as the enthalpy method and the equivalent specific heat method. Here, on the premise that the temperature distribution inside the solidification shell could be approximated by a quadratic expression, it was decided to use the Runge-Kutta method to solve the equation of heat conduction.

The non-steady equation of heat conduction inside the solidification shell is shown below. This equation is used to calculate the temperature distribution from the meniscus to the mold bottom.

$$\frac{\partial T}{\partial t} = \lambda \frac{\partial^2 T}{\partial x^2} \tag{3}$$

where, λ denotes the heat conductivity; T, the solidification shell temperature; and x, the shell thickness direction. Here, as the boundary conditions, it is necessary to set the heat flux (q_0) between the

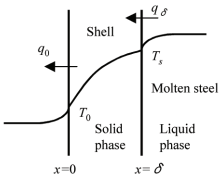

$$x = 0: \quad T = T_0(t) \tag{4}$$

$$\lambda \frac{\partial T}{\partial x} = q_0(t) \tag{5}$$

$$x = \delta: \quad T = T_s \tag{6}$$

$$\lambda \frac{\partial T}{\partial x} = q_\delta(t) + \rho L \frac{d\delta}{dt} \tag{7}$$

Fig. 11 Boundary condition for calculation of solidification

mold and the solidification shell and the heat flux (q_δ) between the molten steel and the solidification shell. The relationship between them is shown in **Fig. 11**. In the figure, λ denotes the heat conductivity; L, the solidification latent heat; δ, the solidification shell thickness; and T_s, the steel solidus temperature; T_0, surface temperature.

(2) Model for FEM analysis of the visco-plastic deformation behavior of the solidification shell

In recognition of the fact that the thickness of the solidified shell in the mold is sufficiently small relative to the slab size and that the temperature distribution in the direction of the solidified shell thickness can be expressed by a relatively simple form, we formulated an FEM model using thick shell calculation elements consisting of four nodes. The shell elements used in the present FEM calculation are illustrated in **Fig. 12**. The temperature distribution and the plastic deformation region were considered at several integration points in the element thickness direction.

The FEM calculations described above made it possible to obtain a three-dimensional analysis taking into consideration mass transfer, phase transformations including solidification, and visco-plastic behavior in the high temperature region.

The formulation of the FEM model is briefly described below. By using the shape function N, the element displacement velocities can be expressed by the following equation.

$$\begin{Bmatrix} \dot{u} \\ \dot{v} \\ \dot{w} \end{Bmatrix} = \sum_{i=1}^{4} N_i \begin{Bmatrix} \dot{u}_i \\ \dot{v}_i \\ \dot{w}_i \end{Bmatrix} + \sum_{i=1}^{4} N_i z \begin{Bmatrix} \dot{\theta}y_i \\ -\dot{\theta}x_i \\ 0 \end{Bmatrix} \tag{8}$$

where, $\dot{u}_i, \dot{v}_i, \dot{w}_i, \dot{\theta}x_i, \dot{\theta}y_i$, and $\dot{\theta}z_i$ denote the displacement velocities and rotational speeds defined at the i^{th} node and z denotes the position in the solidified shell thickness direction. Using the principle of virtual work, the total stiffness equation becomes as follows.

$$[K]\{\dot{u}\} = \{\dot{L}_t\} + \{\dot{L}_T\} + \{\dot{L}_m\} + \{\dot{L}_{vp}\} \tag{9}$$

where, $[K]$ denotes the stiffness matrix and $\{\dot{L}\}$ denotes the nodal force vector. The lower subscripts, t, T, m, and vp, denote the increments of surface force, thermal stress, phase transformation stress, and visco-plastic stress, respectively. Consideration is given to contact and friction between the mold and the solidified shell by adding a spring support.

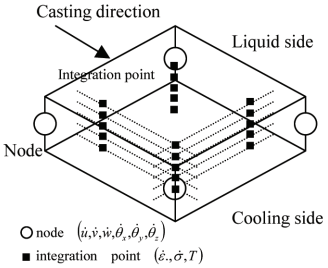

Fig. 12 Thermal-mechanical model for solidifying shell

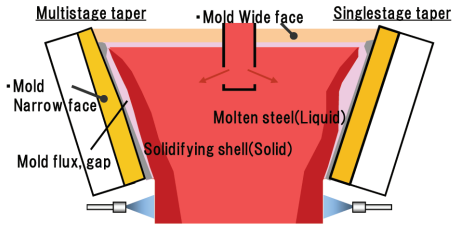

Fig. 13 Shape of mold narrow face and distortion of solidifying shell

The actual calculation procedure is as follows. Apply the temperature distribution obtained by the solidification calculation, described in Section (1) above, to each of the integration points (4 in-plane points + n points in shell thickness direction) within each element. With the stiffness matrix kept unchanged, calculate Equation (9) repeatedly while changing the load velocity vector till the displacement velocity converges. When the displacement velocity converges and the deformation condition can be calculated, the condition of contact between the mold and the solidified shell becomes known. The heat transfer deteriorates at the place where the gap spread, and the heat flux decreases. Taking into consideration the heat flux that has decreased, recalculate the solidification and repeat the above deformation analysis. Thereafter, repeat the procedure until the temperature distribution and shell deformation behavior finally converge.

Using this newly developed model for solidification shell deformation analysis, we analyzed the influence of mold shape on shell solidification and consider to optimize the mold shape, particularly the shape of taper (inclination) of the mold narrow face. It was found that the condition of the formation of a gap (an air gap or a gap filled with powder) between the solidified shell and the narrow-face copper plate changes according to the narrow-face taper shape. As shown in **Fig. 13**, in the case of a narrow face having a single-stage taper shown at right in the figure, the amount of the initial thermal shrinkage of the slab is larger than the amount of taper, whereby a large gap is formed between the shell and the mold. As a result, the solidification of molten steel around the corner is delayed and the solidification shell thickness at the bottom of the mold decreases, causing a crack or BO to occur easily. To solve this problem, a narrow face having a multistage taper has been proposed and put into practical use. Shown at left in Fig. 13 is the narrow face of a mold having a multistage taper, the upper stage having a larger taper than the lower stage. Thus, the amount of taper approaches the amount of thermal shrinkage caused by the initial solidification. As a result, the formation of a gap is restrained and it becomes less likely that a delay in solidification will occur, and consequently, the possibility of defect formation is correspondingly decreased.

The influence of mold taper on solidification shell growth was quantitatively analyzed using the newly developed model. Examples of the analysis results are shown in **Fig. 14**. It was confirmed both by calculations and observations that the multistage taper reduced the amount of gap around the corner and made solidification more uniform. Since the effectiveness of the model was verified, we used the model to design an optimum multistage taper and applied the taper to an actual mold. As a result, the multistage taper made the solidification shell thickness around the corner more uniform than the single-stage taper, and facilitated a more stable, and high-speed continuous casting operation.

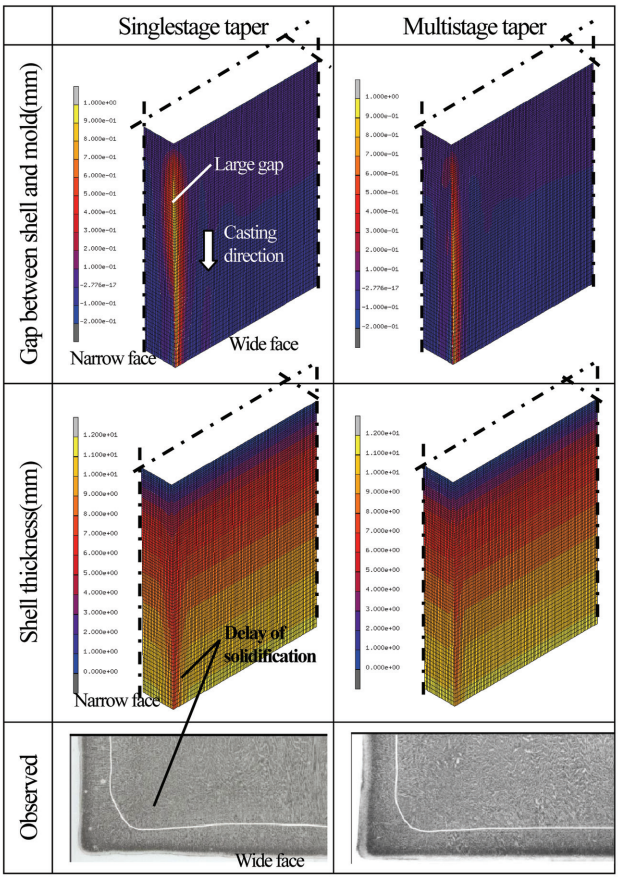

Fig. 14 Evaluation results of multistage taper effect

3.2 Controlling initial solidification by electromagnetic force [23)]

Many steel plates and tubes are made mainly from so-called medium-carbon steel that has undergone hypo-peritectic solidification. It is widely known that, because of the unevenness of initial solidification shell produced by the process, a longitudinal crack tends to occur easily in the slab of medium-carbon steel. Application of electromagnetic stirring (EMS) to the molten steel in the mold is known to be effective at reducing the formation of longitudinal cracks in the slab. However, the effect of EMS on the solidification shell is not completely understood. Therefore, we studied the effect of EMS on the uniformity of the initial solidification shell. The difference in the molten steel temperature distribution between EMS on and EMS off conditions is shown in **Fig. 15**, and the difference in the solidified shell thickness distribution between EMS on and EMS off conditions is shown in **Fig. 16**.

When EMS is applied, the turbulent flow of molten steel into the mold, which is caused by the immersion nozzle discharge flow, becomes a stable, swirling flow. As a result, it is suggested that, with the application of EMS, the fluctuation in temperature of the molten steel in the mold decreases, the molten steel temperature distribution becomes more uniform, the mold flux melts more stably, and the infiltration of molten flux stabilizes. All this is considered to help reduce the fluctuation in heat flux in the mold and stabilize the initial solidification.

The above mechanism was confirmed by a magnetohydrodynamics simulation coupled with a solidification analysis. Thus, it was found that when EMS is applied to give a molten steel flow at

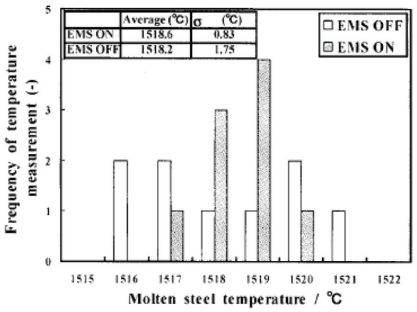

Fig. 15 Molten steel temperature in the mold

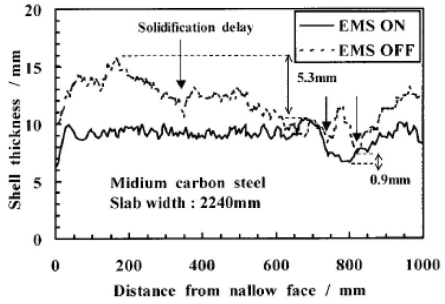

Fig. 16 Distribution of shell thickness in width direction

the front of the solidification interface, the fluctuation in solidification shell thickness decreases and the initial solidification becomes more uniform.

3.3 Controlling solidification in strand by secondary cooling [24)]

In the secondary cooling zone of the strand, the roll pitch is reduced so as to support the thin shell of the slab during high-speed casting, and hence, small-diameter rolls are used. Unfortunately, small-diameter rolls are inferior in stiffness and tend to be deformed easily. Therefore, rolls split into several segments across the width are generally used. In this case, however, since several bearings need to be provided across the roll width, it is expected that spray water, used for cooling the slab, flows downstream along the bearings in an irregular fashion. In order to analyze the influence of the irregular flow of spray water on uneven solidification, it is important to quantitatively grasp the behavior of spray water flow. Although a flow analysis is effective for that purpose, it is difficult to apply the conventional method of flow analysis using meshes to handle a complicated free surface. Therefore, we considered applying the particle method, which does not use meshes.

Focusing upon the characteristic roll set in the secondary cooling zone, the behavior of cooling water was analyzed using a model consisting of five stages of rolls in the casting direction and four stages of sprays between them. The particle method (MPS)[25)] was applied in the calculations, and general-purpose software[26)] added with certain functions was used in the analysis. As a result, it was found that, depending on the flow rate of spray water, the cooling water that is sprayed onto the slab flows (drips) downstream irregularly through the bearings and is accumulated between the downstream roll and the slab and eventually overflows the roll as shown in **Fig. 17**. The accuracy of the above model was verified by using a water model. The usefulness of the calculation model was confirmed by comparing calculated and measured flow rates of water flowing through the bearings and slab edge.

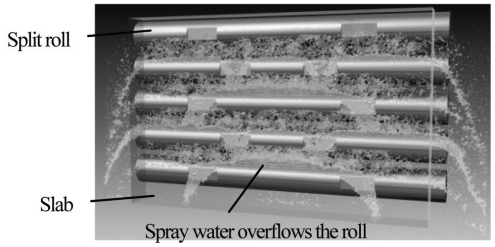

Fig. 17 Calculated result of spray water flow (view from slab side)

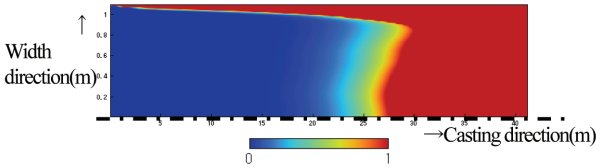

Fig. 18 Solid fraction at center of thickness

A thorough understanding of the phenomenon of shell solidification in the strand requires performing a solidification calculation taking into consideration the irregular flow of spray water mentioned above. Although many measurements of the heat transfer coefficient for a spray proper have been made in the past, a quantitative study has seldom been made on the cooling of a slab by dripping water or a pool of water on the roll. Therefore, we carried out an experiment in which a steel plate in which several thermocouples were implanted was heated and cooled by dripping water and pooled water, simulative of the secondary cooling zone of the strand, to measure the heat transfer coefficient. With consideration given to the effect of the bearing arrangement on the behavior of dripping water, the shell solidification calculation was conducted by applying the experimentally derived temperature distribution to the heat transfer coefficient in the casting direction and across the width. The results of the calculation are shown in **Fig. 18**.

As can be seen from Fig. 18, solidification across the slab width becomes uneven owing to the intense cooling at the center of the slab width, with the result that the center of the slab thickness solidifies first. It is very likely that this uneven solidification promotes the W-shape solidification that is considered to foster centerline segregation. The arrangement of the bearings, the spray geometry, and the flow rate of spray water influence the occurrence of dripping water. When the flow rate of spray water is high during high-speed continuous casting, etc. Therefore, it is necessary to consider this phenomenon during the design of high-speed continuous casting equipment and operation conditions.

4. Conclusion

The phenomenon of heat transfer in the mold and the strand has been quantitatively evaluated and technology for controlling the phenomenon has been examined. As a result, the following facts were ascertained.

- In the heat transfer through mold flux film, the interfacial resistance predominates when the film is thin, whereas the thermal resistance of the solidified layer predominates when the film is thick.
- The infiltration of mold flux occurs during the period from the second half of the positive strip time till the second half of the negative strip time. The amount of flux infiltration increases

with a decrease in viscosity, casting speed, and oscillation frequency.

- Hydrogen-induced breakout is caused by micropores that occur when the amount of OH^- in the mold flux increases. In order to prevent breakouts, it is effective to use a flux of high basicity and reduce the hydrogen concentration of the molten steel.
- The magnitude of the air gap between the mold and the solidifying shell varies according to the mold shape. By applying a multistage taper to the mold narrow face, it is possible to improve the uniformity of the solidified shell.
- Electromagnetic stirring of the molten steel in the mold promotes a uniform distribution of molten steel temperature, which helps improve the uniformity of the initial solidification shell.
- Irregular spray water flow between roll bearings and the water pooled between the roll and the slab adversely affect the widthwise uniformity of the solidifying shell.

References

1) Mineta, S. et al.: CAMP-ISIJ. 23, 985 (2010)
2) Yamauchi, A. et al.: Tetsu-to-Hagané. 79, 167 (1993)
3) Watanabe, K. et al.: Tetsu-to-Hagané. 83, 115 (1997)
4) Cho, J. et al.: ISIJ International. 38, 440 (1998)
5) Fukuda, J. et al.: CAMP-ISIJ. 5, 281 (1992)
6) Hanao, M. et al.: Tetsu-to-Hagané. 92, 655 (2006)
7) Kajitani, T. et al.: ISIJ International. 48, 1215 (2008)
8) Kajitani, T. et al.: ISIJ International. 46, 250 (2006)
9) Kajitani, T. et al.: ISIJ International. 46, 1432 (2006)
10) Okazawa, K. et al.: ISIJ International. 46, 226 (2006)
11) Okazawa, K. et al.: ISIJ International. 46, 234 (2006)
12) Emi, T. et al.: 61st National Open Hearth Basic Oxygen Steel Conf. Proc. ISS/AIME, Warrendale, PA, 1978, p. 350
13) Kitagawa, T. et al.: Trans. Iron Steel Inst. Jpn. B-173 (1980)
14) Anzai, E. et al.: Nippon Steel Technical Report. (34), 31 (1987)
15) Itoyama, S. et al.: CAMP-ISIJ. 9, 74 (1996)
16) Kajitani, T. et al.: ISIJ International. 48, 1215 (2008)
17) Zasowski, P. J. et al.: 73rd Steelmaking Conf. Proc. ISS/AIME, Warrendale, PA, 1990, p. 253
18) Pontoire, J. N. et al.: Rev. Metall. 36 (2000)
19) Mizukami, H. et al.: ISIJ International. 44, 1714 (2004)
20) Saito, K. et al.: Annu. Rep. NMR Spectrosc. 44, 23 (2001)
21) Ueshima, Y. et al.: Tetsu-to-Hagané. 98, (2012), in press
22) Wan, S. et al.: Trans. Japan Society of Mechanical Engineers (A). 53, 1739 (1987)
23) Nakashiima, J. et al.: Tetsu-to-Hagané. 93, 565 (2007)
24) Yamasaki, N. et al.: CAMP-ISIJ. 25, 264 (2012)
25) Koshizuka, S. et al.: Ryushiho (The Particle Method). Maruzen Publishing Co., 2005
26) Prometech Software, Inc., Particleworks

Hideaki YAMAMURA
Chief Researcher
Steelmaking R&D Div.
Process Technology Center
20-1 Shintomi, Futtsu, Chiba 293-8511

Norimasa YAMASAKI
Department Manager
Mechanical Engineering Div.
Plant Engineering and Facility Management Center

Toshiyuki KAJITANI
Manager, Dr.Eng.
Technical Development Planning Div.

Satoru MINETA
Researcher
Steelmaking R&D Div.
Process Technology Center

Junji NAKASHIMA
Chief Researcher, Dr.Eng.
Steelmaking R&D Div.
Process Technology Center